Calculations of the mass absorption cross sections for carbonaceous nanoparticles modeling soot

C. García Fernández, Sylvain Picaud, M. Devel

Calculations of the Mass Absorption Cross Sections for carbonaceous nanoparticles modeling soot

C. García Fernández

Institut UTINAM-UMR CNRS 6213, Université de Franche-Comté
16 route de GRAY, F-25030 Besançon Cedex, France.

Instituto Superior de Tecnologias y Ciencias Aplicadas (InSTEC), Ave. Salvador Allende y Luaces, Quinta de los Molinos Plaza, Habana 10600, Cuba

S. Picaud

Institut UTINAM-UMR CNRS 6213, Université de Franche-Comté
16 route de GRAY, F-25030 Besançon Cedex, France.

M. Devel

Institut FEMTO-ST UMR 6274 CNRS/Université Franche-Comté, ENSMM, UTBM
Temis Science, 15 B av. des Montboucons, F-25030 Besançon Cedex, France.

Abstract

In this paper we use an atomistic model to calculate the mass specific absorption cross section coefficient of carbonaceous particles of nanometer size. The carbonaceous particles are built numerically to reproduce most of the structural characteristics of typical **primary nanoparticles that are agglomerated in soot** emitted in the Troposphere from combustion sources. Our model is based on the knowledge of the atomic positions and polarizabilities inside the **primary nanoparticles** and is used to study the influence of these atomistic characteristics on the optical properties of these nanoparticles. The results indicate that the atomistic composition of the soot **primary nanoparticles** may have a sufficiently strong impact on the **mass specific absorption cross section coefficient (MAC)** curves to allow detection of differences between nanoparticles by using UV-visible spectroscopic measurements, in a well-suited wavelength range, i.e., typically between 200 and 350 nm. In a more general way, our calculations show that MAC values as well as differences between MAC curves corresponding to different **primary nanoparticles** may strongly vary with wavelength. As a consequence, measurements at a given wavelength only are certainly not representative of the absorption properties of these nanoparticles and thus should be considered with caution. **Moreover, our approach clearly shows significant differences with classical macroscopic electromagnetic theory when calculating the optical properties of realistic primary soot nanoparticles that, in fact, cannot be considered as homogeneous spherical particles due to the presence of defects in their atomistic structure.**

Email address: sylvain.picaud@univ-fcomte.fr (S. Picaud)

Keywords: Absorption cross section, carbon soot, optical properties, modeling
PACS: 42.68.Mj, 81.05.Rm, 33.15.Kr, 61.48.-c

1. Introduction

Carbonaceous particles emitted by combustion processes are suspected to have a non-negligible impact on the Earth's radiative balance[1]. First, they have direct effects because they scatter and absorb solar and thermal infrared radiation, thus modifying the Earth's albedo. Second, they have an indirect effect because these particles may act as ice and cloud condensation nuclei thus impacting on the local and global radiative properties of clouds[2, 3]. These particles, together with the other atmospheric aerosols, are currently one of the largest sources of uncertainties in understanding climate evolution and in quantifying the amplitude of temperature changes[4]. This mainly comes from the high natural variability of the sources of carbonaceous particles due to different conditions of combustion and fuel compositions[5].

In a general way, carbonaceous particles consist of a complex mixture of chemical compounds and are usually divided into two fractions. The black (or elemental) carbon (BC) fraction is a strong absorber of visible and near-IR light and BC concentrations therefore are usually determined by light-absorption measurements. In contrast, the organic fraction (OC) of the aerosol represents an aggregate of hundreds of individual compounds exhibiting a wide range of chemical and thermodynamic properties. Because of this complexity, aerosol OC content is usually determined from the difference between total carbon and BC contents[5]

Widely accepted structural models for BC combustion particles are based on their fractal character coming from agglomeration of primary carbonaceous nanoparticles. These models assume that the primary nanoparticles are made of graphene sheets, whose stacking on concentric spheres of different radii results in typical onion-like structures[6]. These primary nanoparticles may also contain a very small fraction of other atoms (mainly oxygen) besides carbon, due to partial oxidation[7]. They also contain defects like edges or atom vacancies formed during the recombination of soot precursors,[8], leading thus to different ratios of aromatic to aliphatic carbon atoms.

Owing to this complexity, a detailed understanding of both direct and indirect climatic effects of carbonaceous particles remains challenging and requires the characterization of the interaction of these particles with electromagnetic radiations, as a function of the geometrical and chemical characteristics of the nanoparticles constituting the carbonaceous fraction of the aerosols.

In this respect, theoretical approaches at the atomic scale can give details on the involved processes that are not directly accessible to experimental probes. They can also help at interpreting experimental information and data coming from observations.

In a recent series of papers[9, 10, 11, 12], we have thus modeled soot surfaces and their interaction with water to characterize the influence of the structural and chemical details on the ability of soot nanoparticles to act as ice and cloud condensation nuclei (indirect effect on climate). Here, we rather focus on the direct effect on climate, i.e., on the relation between the soot nanostructure and its interaction with solar radiation, on the basis of a preliminary work[13, 14].

Indeed, athough the study of light absorption by carbonaceous particles is not a new field (see for instance the reviews by Sorensen[15] and Bond et al.[16]), a direct relation between the atomistic

characteristics of these particles and their effect on climate is still missing. For instance, simplified macroscopic models are still widely used based on the Mie theory[17, 18], that generally assumes single (or aggregates of) homogeneous spherical particles. More sophisticated approaches are also able to take into account heterogeneity[19, 20] or irregularly shaped particles[21]. On the same way, powerful numerical methods such as the discrete dipole approximation (DDA)[22, 23, 24] or the T-matrix[25] are now largely disseminated for computing scattering of radiation by particles of arbitrary shape and by periodic structures. However, none of these methods allows a direct connection between the atomic composition of carbonaceous particles and their absorption/extinction properties. Here, we present a method to calculate the absorption properties of carbonaceous nanoparticles that is directly based on the knowledge of the positions and polarizability of the atoms constituting the particle. This method, **based on the point dipole interaction model (PDI)[26]**, is more specifically used to calculate the mass specific absorption cross section coefficient (MAC) of **primary soot nanoparticles** modeled at the atomic scale and is described in Section 2. Then, the accuracy of the parameters used to represent the carbon atom polarizability is checked by comparison with experimental results obtained for the C_{60} molecule in Section 3. In the same section, the results for fullerene molecules of increasing radius are also given to investigate the influence of the particle size on the MAC calculations. In Section 4, the approach used to model primary soot nanoparticles at the atomic scale is detailed and the corresponding MAC curves are calculated in the UV spectral range. Finally, conclusions are given and further developments of this work are discussed in Section 5.

2. Model

Here, we chose to calculate two experimentaly relevant properties, i.e., the absorption cross section C_{abs} and the mass specific absorption cross section coefficient (MAC) defined as the ratio of C_{abs} to the total mass of the nanostructure.

Following the work of Draine[23], C_{abs} for a nanograin made of N atoms can be related to the imaginary part of the dynamic polarizability tensor $\overleftrightarrow{\alpha}_i(\omega)$ of each atom i as[23] :

$$C_{abs}(\omega) = \frac{4\pi k}{|E_0(\omega)|^2} \sum_{i=1}^{N} \left\{ Im[\vec{\mu}_i(\omega).(\alpha_i^{-1}(\omega))^* \vec{\mu}_i(\omega)^*] - \frac{2}{3} k^3 \vec{\mu}_i(\omega).\vec{\mu}_i(\omega)^* \right\}, \quad (1)$$

where $\vec{\mu}_i$ represents the induced dipole moment on the ith atom and $k = 2\pi/\lambda$ is the wavenumber associated to the incident light of wavelength λ. $|E_0(\omega)|$ is the amplitude of an external plane wave.

To calculate $\vec{\mu}_i$, we used the Point Dipole Interaction (PDI) model[26] in which this dipole can be directly computed from the knowledge of the atomic polarizabilities and of the local electric field $\vec{E}_{loc}(\vec{r}_i, \omega)$ at position $\vec{r}_i$.

Note that the PDI model is in fact similar to the discrete dipole approximation (DDA) method[22, 23, 24]. However, DDA is used at the microscopic scale with effective polarizabilities that are derived from a combination of the material local dielectric susceptibility and the volume of discretization elements. As a consequence, DDA is based on a ClausiusMossotti-like relation (with radiative corrections) between the relative dielectric constant of the material and the effective polarizability of the

discretization volumes. In contrast, as it will be explained below, PDI requires the knowledge of the exact positions $\vec{r}_i$ of the atoms constituting the nanostructure under investigation and of their polarizabilities. Note that these atomic polarizabilities can either be derived from *ab initio* Time Dependent Density Functional Theory (TD-DFT) calculations or from ClausiusMossotti-like relations but with depolarization factors adapted to the symetries of the true atomic lattice and not to a rhomboedral lattice discretization.

In the PDI model, the local electric field is thus written as in DDA, as the sum of the external field $\vec{E}_0(\omega)$ and of the electric field created at the position $\vec{r}_i$ by the dipoles induced on the other atoms of the carbonaceous nanostructure. Hence, the individual dipoles can be computed by solving the following linear system of equations:

$$\forall i = 1, ..., N \quad \vec{\mu}_i, (\omega) = \overset{\leftrightarrow}{\alpha}_i\ (\omega)\vec{E}_0(\omega) + \sum_{j \neq i=1}^{N} \overset{\leftrightarrow}{\alpha}_i\ (\omega)\ \overset{\leftrightarrow(2)}{T}\ (\vec{r}_i, \vec{r}_j, \omega)\vec{\mu}_j(\omega)\ , \tag{2}$$

where $\overset{\leftrightarrow(2)}{T}$ is the electric field propagator in vacuum that is written as[14]

$$\overset{\leftrightarrow(2)}{T}\ (\vec{r}_i, \vec{r}_j, \omega) = -\frac{1}{\epsilon_0}\left(\vec{\nabla}_{\vec{r}_i} \otimes \vec{\nabla}_{\vec{r}_i} + \frac{\omega^2}{c^2}\ \overset{\leftrightarrow}{\mathbb{I}}\right)\left(-\frac{e^{i\frac{\omega}{c}|\vec{r}_i - \vec{r}_j|}}{4\pi\,|\vec{r}_i - \vec{r}_j|}\right), \tag{3}$$

where $\overset{\leftrightarrow}{\mathbb{I}}$ is the (3×3) identity matrix.

The calculation of the absorption cross section for the carbonaceous nanostructures considered here thus requires the knowledge of the exact positions $\vec{r}_i$ of the atoms constituting this nanostructure. In this respect, the PDI method thus differs from the usual implementations of the Discrete Dipole Approximation (DDA) method [22, 23] that are rather based on the scattering of dipoles on a regular cartesien grid to allow use of fast Fourier transform algorithms. Note that despite this arbitrary discretization of the volume of the nanostructure under consideration, DDA approaches are much often used in the literature especially because of the wide dissemination of corresponding open source codes[24, 27, 28, 29], in contrast to the PDI method for which no general code is available. As the exact atomic positions are often not known in many carbonaceous structures, especially the soot systems investigated here, the PDI method thus could appear irrelevant at first sight. However, these positions can be defined in model systems such as the one used here (see below) and the exact relation between the optical properties of a carbonaceous nanostructure and its atomic details can be directly computed, without any assumption on the global geometry of the system under study. In a similar way, combining this PDI approach with experimental measurements could allow optical methods to be an unique probe for examining the intimate structure of such carbonaceous systems.

Eq. 2 also requires the knowledge of the atomic tensors $\overset{\leftrightarrow}{\alpha}_i\ (\omega)$ associated to the atoms present in the nanostructure under study. Considering that the carbonaceous nanostructures investigated here can *a priori* be made of different hybridized carbon atoms (depending on the local environment of the carbon atoms in the system) we have to define different atomic polarizability tensors for the corresponding C atoms.

Here, we consider that carbon atoms that are surrounded by three nearest neighbors can be treated as sp2 hybridized carbons. Their representation is thus simple in a local frame defined by two unit vectors parallel to the plane defined by the three nearest neighbors of the considered atom and one unit vector perpendicular to this plane[30]. Indeed, in this local frame, the atomic polarizability tensors are diagonal (and anisotropic) with two parallel components ($\alpha_{i,||}^{local}$) and one perpendicular component ($\alpha_{i,\perp}^{local}$). For coherence with our previous works[13, 14], we use here a convention which is at the opposite of that usually used for graphite in which perpendicular and parallel directions are defined with respect to the c-axis (perpendicular thus usually means parallel to the graphite surface plane, whereas here it means perpendicular to the local plane of 3 nearest neighbors).

The atomic polarizability tensors can then be computed in the nanostructure global frame $(\vec{u}_x; \vec{u}_y; \vec{u}_z)$ by simple geometric transformations, as:

$$\overleftrightarrow{\alpha}_i = R^{-1} \overleftrightarrow{\alpha}_i^{local} (\omega) \cdot R \tag{4}$$

by using the rotation matrix R that connects the local to the global frame.

However, carbonaceous nanostructures may also contain C atoms that are not surrounded by three carbons. For instance, C atoms located at boundary sites or at defect edges of the nanostructure may have only one or two carbon neighbors. For these atoms, which cannot be considered at all as sp2 hybridized carbons, we rather defined isotropic polarizability tensors, characterized in a first approximation by the value $\alpha_i^{iso} = (2\alpha_{i,||}^{local} + \alpha_{i,\perp}^{local})/3$.

3. Results for fullerences

3.1. Parameters and validation

Here, we are interested in computing the optical properties of carbonaceous nanostructures modeling soot nanoparticles. As mentioned above, this requires the prior knowledge of the atomic polarizability tensors $\overleftrightarrow{\alpha}_i (\omega)$ associated to the C atoms forming the nanoparticles, and thus depends on the values assigned to the ($\alpha_{i,||}^{local}$) and $\alpha_{i,\perp}^{local}$ components. In addition, the polarizability tensors may be isotropic or anisotropic depending on the local neighboring of the C atoms (i.e., depending, in our approach, on the number of next neighbor C atoms).

To calculate these polarizability tensors, we have used different sets of dielectric constant values available in the literature for carbon atoms in graphite[31, 32, 33, 34], the conversion from dielectric constant to polarizability being done using the generalized Clausius−Mossotti relation as:

$$\frac{N}{V} \frac{\alpha_{i,a}^{local}(\omega)}{\epsilon_0} = \frac{\epsilon_{i,a}(\omega) - 1}{1 + B_a(\epsilon_{i,a}(\omega) - 1)} \quad . \tag{5}$$

where the index a labels one of the three principal directions defining the local basis frame and N/V is the atomic density. The coefficients B_a are the depolarization factors assumed here to be equal to those of graphite, i.e., $B_\perp = -0.606$ and $B_{//} = 0.803$ [35, 36]. Note that taking $B_\perp = B_{//} = \frac{1}{3}$ in Eq. 5 would lead to the usual Clausius−Mossotti relation.

Of course, these dielectric constant values (and thus, the polarizability values used here) have been optimized for graphite and their application to soot could be questionable although soot nanoparticles are actually made of graphite-like nanoclusters[6].

Thus, to investigate the transferability of these parameters to round shaped nanostructures such as soot nanoparticles, we have calculated the polarizability per unit volume of C_{60} and C_{70} fullerenes using the three sets of parameters. This calculation has been based on the PDI approach[26], where the polarizability of the carbonaceous nanostructure is directly computed from the knowledge of the atomic polarizabilities through the following equations[13, 14] :

$$\vec{\mu}(\omega) = \overleftrightarrow{\alpha}\ (\omega)\vec{E_0}(\omega) = \sum_{i=1}^{N} \vec{\mu}_i(\omega) = \sum_{i=1}^{N} \overleftrightarrow{\alpha}_i\ (\omega)\vec{E}_{loc}(\vec{r}_i, \omega) \tag{6}$$

where $\vec{\mu}$ is the total electrical dipole moment of the carbonaceous nanostructure, $\overleftrightarrow{\alpha}\ (\omega)$ is the dynamical polarizability tensor of the carbonaceous nanostructure containing N carbon atoms and $\vec{E_0}(\omega)$ is the external electric field applied to the system. $\vec{\mu}_i$ is the dipole induced on atom i by the local electric field $\vec{E}_{loc}(\vec{r}_i, \omega)$ at its location $\vec{r}_i$ (Eq. 2). $\overleftrightarrow{\alpha}_i$ defines the dynamical polarizability tensor of atom i calculated as mentioned above using parameters coming from graphite data. Then, imposing an unit field $\vec{E_0}$ successively along the three coordinate axes $(\vec{u}_x, \vec{u}_y; \vec{u}_z)$ of the global frame, we can easily get the three columns of the polarizability tensor $\overleftrightarrow{\alpha}$ of the carbonaceous nanostructure from Eq. 6.

The application of graphite data to predict properties of fullerenes has been already discussed in detail by Andersen and Bonderup[36] which pointed out some inconsistency between various sets of data, especially concerning the values for $\epsilon_\perp$. However, due to the lack of any reliable set of parameters specially suited for carbon atoms in curved structures such as soot nanoparticles, using parameters optimized for graphite still remains unavoidable.

The polarizability values calculated with the three selected sets of parameters have then been used to determine the function $\mathrm{Im}(-1/\epsilon)$, through the usual Clausius−Mossotti relation, considering in the calculations that C_{60} and C_{70} fullerenes are arranged in a face-centered cubic structure based on lattice parameters $a = 14.117$ Å and $a = 14.9$ Å, respectively. This aimed at directly comparing our results to the experimental loss function of C_{60} and C_{70} crystals as obtained by Sohmen et al.[37] in an Electron Energy Loss Spectroscopy experiment.

The theoretical curves are given in Fig 1 for both C_{60} (Fig 1a) and C_{70} (Fig 1b) fullerenes together with the corresponding experimental curves [37] for comparison. The theoretical curves in Fig 1 exhibit two broad peaks that can be related to the experimental peaks characterizing collective excitations of valence electrons. For the two fullerenes considered here, the first peak (corresponding to π plasmon[38]) has its maximum between 6 and 7 eV, whereas for the second peak (which corresponds to $\sigma + \pi$ plasmon[38]) the maximum is obtained between 22 and 28 eV, depending on the parametrization that is used in the calculations.

The comparison with the experimental curves shows that the three different parametrizations used here appear to be quite relevant for describing the features below 8 eV. However, the results obtained with the parameters given by Draine et al[31, 32, 33] seems slightly more accurate than those issued from Djurisic's work[34]. In contrast, theoretical results obtained by using optical constants coming from EELS and ellipsometry[34] seems to better reproduce the experimental

features above 8 eV, although a small shift (of around 2 eV) is evidenced for the maximum position of the main peak. Note that, as expected, some resonances related to excitations from π to π^* orbitals for the C_{60} and C_{70} crystals (peaks below 5 eV) [39] cannot be accounted for by any parametrization optimized for graphite where such transitions are not possible due to symmetry considerations.

To conclude, it appears that the parameters given by Draine et al.[31, 32, 33] for graphite can also be used with reasonable confidence to get at least qualitative results for fullerenes, and more generally spherical carbonaceous particles[20, 36], especially when restricting the calculations to the near UV zone, as in the following.

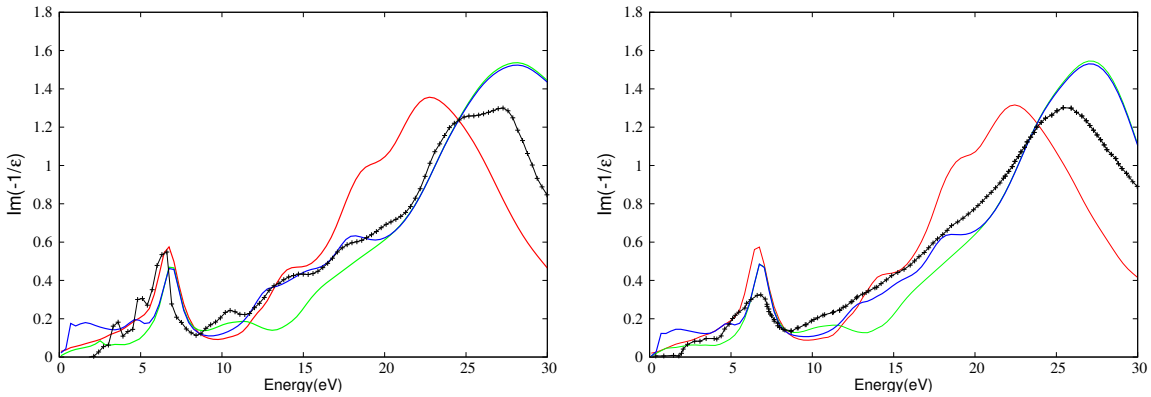

Figure 1: Comparison between the experimental Loss function Im$(-1/\epsilon)$ (black curve) for a cristal of (a) C_{60} and (b) C_{70} [37] and the theoretical curves computed with three different sets of optical constants derived from graphite data; red, green and blue curves correspond to parametrizations from Ref.[31, 32, 33] and Ref.[34] (for optical and for EELS data), respectively.

3.2. Fullerenes of increasing radius

In this section we have simulated the interaction of single fullerenes with light to calculate their optical properties in the near UV zone, as a function of their increasing size. As the extinction cross section is mainly dominated by absorption, we first seek to compare the photoabsorption cross section C_{abs} for a C_{60} fullerene with the experimental data reported in the literature[40, 41] before extending the study to larger fullerenes. The comparison given in Fig 2 between our theoretical results and the experimental curve shows that our approach reproduces quite well the main peack position around 6 eV, as already evidenced in the previous section when calculating Im$(-1/\epsilon)$. Again this figure points out that calculations based on the optical constants derived from graphite data cannot reproduce some of the C_{60} resonances below 5 eV.

We then extended our calculations to larger fullerenes, considering C_{240}, C_{540}, C_{960} that are icosahedral fullerenes like C_{60} and including also C_{180}, C_{320} and C_{1280} that are triacontahedral fullerenes.The corresponding results are given in Fig 3 in the near UV to visible range, i.e., typically between 150 and 550 nm (corresponding to the [2.3 - 8.3] eV range). Note that we choose here to use nm for the MAC curves for coherence with the corresponding literature.

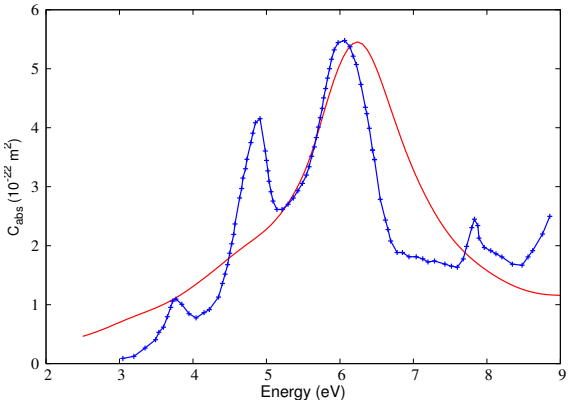

Figure 2: Comparison between the photoabsorption cross section calculated for a C_{60} fullerene (red curve) and that reported by [41] (blue curve). Calculations have been performed by using the graphite optical constants given by Draine *et al.*[31, 32, 33].

The curves in Fig 3 show that the maximum position of the resonance peak is shifted to high wavelength values (by about 45 nm) and that its maximum intensity increases when the size of the fullerenes increases. An interesting consequence of these two features is that for wavelengths lower than approximately 200 nm the mass specific absorption cross section (MAC) of fullerenes decreases with their radius, whereas it increases for larger wavelengths.

These results are in accordance with those of previous works that used either a simplified model[42] or an approach based on the PDI method[43] for the calculations of dynamical polarizabilities of fullerenes, but limited to energies lower than the first electronic excitation energy.

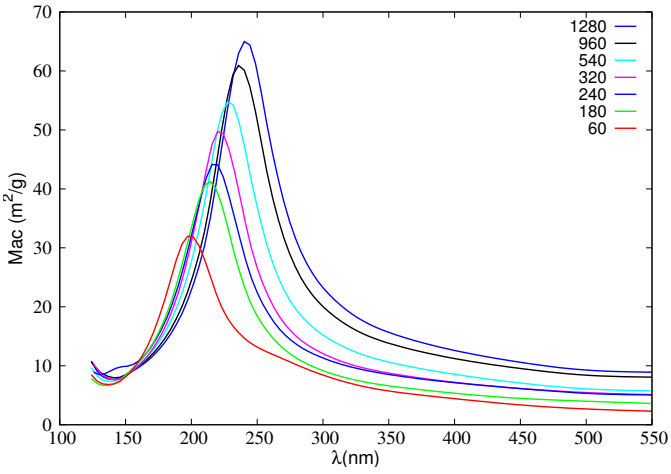

Figure 3: Computed mass absorption cross section (MAC) for the icosahedral C_{60},C_{240},C_{540},C_{960} and the triacontahedral C_{180}, C_{320},C_{1280} fullerenes.

Because in our model we can use either isotropic or anisotropic polarizability tensors to describe C atoms, depending for instance on their number of neighbors, it was interesting to study the

influence of such a choice on the MAC curves calculated for different fullerenes. Of course, in such structures, the C atoms are all surrounded by 3 neighbors as in graphite, and considering that they could be represented by isotropic polarizability may appear surprising at first sight. Nevertheless, this allows the characterization of the influence of the parametrization on our results by comparing MAC curves obtained for the same nanostructure but for two different representations of the polarizability tensors of the C atoms.

As an illustration, the corresponding results are given in Fig 4 for the smallest (C_{60}) and the largest (C_{1280}) fullerenes considered here.

Interestingly, for C_{60}, both isotropic and anisotropic polarizability tensors give similar MAC curves, especially when considering the position of the resonance peak around 200 nm. In contrast, for C_{1280}, not only strong differences in the MAC intensity but also a large shift of the resonance peak (of about 30 nm) are obtained when using different hypotheses for the polarizability tensor of the C atoms. This could be related to the fact that, for such large fullerene, each C atom and its three nearest neighbors are approximately located in the same plane, as in graphite, thus enhancing the influence of the differences between isotropic and anisotropic parametrization. Moreover, this indicates that, at least in our approach and for large structures, sp2-hybridized carbon atoms will lead to much stronger absorption than C atoms represented by isotropic polarizabilities resulting from an average of the anisotropic values. Interestingly, this could give us an useful tool to discriminate between strongly and weakly absorbing carbons in further modeling, and thus would help, for instance, at representing the differences experimentally evidenced between elemental and organic carbons[44].

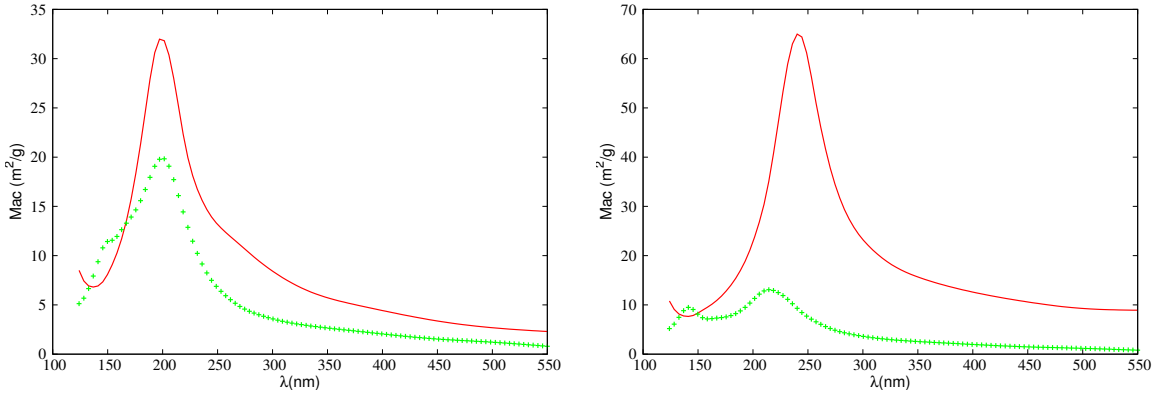

(a) C_{60} (b) C_{1280}

Figure 4: Computed mass absorption cross section (MAC, in m^2/g) obtained when using isotropic (green curve) and anisotropic (red curve) atomic polarizabilities for (a) C_{60} and (b) C_{1280} fullerenes.

4. Results for soot nanoparticles

4.1. soot nanoparticle models

The results presented above have shown that parameters optimized for graphite can reasonably well reproduce the optical properties of fullerenes, in accordance with previous conclusions[20, 36].

The transferability of these parameters to various carbonaceous systems can thus justify using them for modeling the MAC of soot nanoparticles. As mentioned above, calculating the MAC with the PDI approach requires not only the knowledge of the atomic polarizabilities (taken here as equal to those of carbons in graphite) but also of the atom positions in the carbonaceous nanostructures.

We have thus modeled here four different **primary soot nanoparticles**, on the basis of our previous works devoted to water adsorption on soot[9, 12]. Such approach allows us to evaluate qualitatively the dependence of soot optical properties on particle morphology at the atomic scale.

The first nanoparticle is generated by randomly scattering small clusters of 19 carbon atoms on concentric spheres arranged in an onion-like structure[9]. This small cluster, referred below as the C_{19} unit, is made of five fused benzene rings. One hundred and thirteen of these C_{19} units (corresponding to a total number of 2147 carbon atoms) have been randomly scattered on the surface of four concentric spheres of increasing radii (from 9.6 to 20.7 Å), the separation between two successive spheres being equal to 3.4 Å, in accordance with experimental observations for combustion soot [45]. For the scattering of the C_{19} units on the surface of these spheres, a minimum distance of 3.80 Å has been imposed between the nearest neighboring carbon atoms of two adjacent units on the same sphere. The relative orientation of two adjacent C_{19} units has been randomly distributed. The corresponding **primary soot nanoparticle**, referred hereafter as the S_{units} nanoparticle is shown in Fig. 5a.

In addition to this empirically generated **primary soot nanoparticle**, we have built three other nanoparticles starting from the optimized structures of carbon buckyonions (i.e., multi-shell fullerenes) containing four carbon layers arranged in a concentric way just as S_{units}.

Moreover, to model the presence of holes and nanopores in the (defective) structure of **primary soot nanoparticles**, C atoms have been randomly removed from the initial buckyonion structure. Then, the resulting structures have been relaxed in a molecular dynamics simulation run performed at 298 K on the canonical N,V,T, ensemble, in which the adaptative intermolecular reactive empirical bond order (AIREBO) potential has been used to describe the carbon–carbon interactions[46].

It is worth noting that the corresponding structures are thus not based on a random scattering of units of same size (as S_{units}) but rather on a random distribution of holes. These particles will be referred below as S_{holes} nanoparticles.

Two of these S_{holes} nanoparticles have been based on the structure of the four-shell fullerene $C240@C540@C960@C1500$, relaxed after removing 1033 and 1107 carbon atoms, respectively, to model different localization of carbon atoms in similar structures . They contain 2207 and 2133 carbon atoms respectively, and are characterized by an external radius of about 22 Å. These S_{holes} nanoparticles are thus similar to S_{units} with respect to the total number of C atoms, although they are slightly larger in size. The main difference comes from the size of the internal cavity, which is determined here by the radius of the smallest fullerene (C_{240}) embedded in the buckyonion. It it indeed twice smaller for the two S_{holes} (radius value equal to about 4.3 Å) than for the S_{units} nanoparticles (radius value equal to about 9.6 Å). We thus built a third S_{holes} nanoparticle based on the structure of the larger four-shell $C540@C960@C1500@C2160$ fullerene, i.e., a buckyonion that is characterized by an internal cavity of size similar to the one in S_{units}, but that contains a much larger number of C atoms. However, it was not possible to get any stable structure when removing a too large number of atoms in this buckyonion and thus we choose to model a S_{holes} nanoparticle

containing 3774 carbon atoms. The relaxed structures of the three S_{holes} nanoparticles are shown in Fig. 5b,c,d.

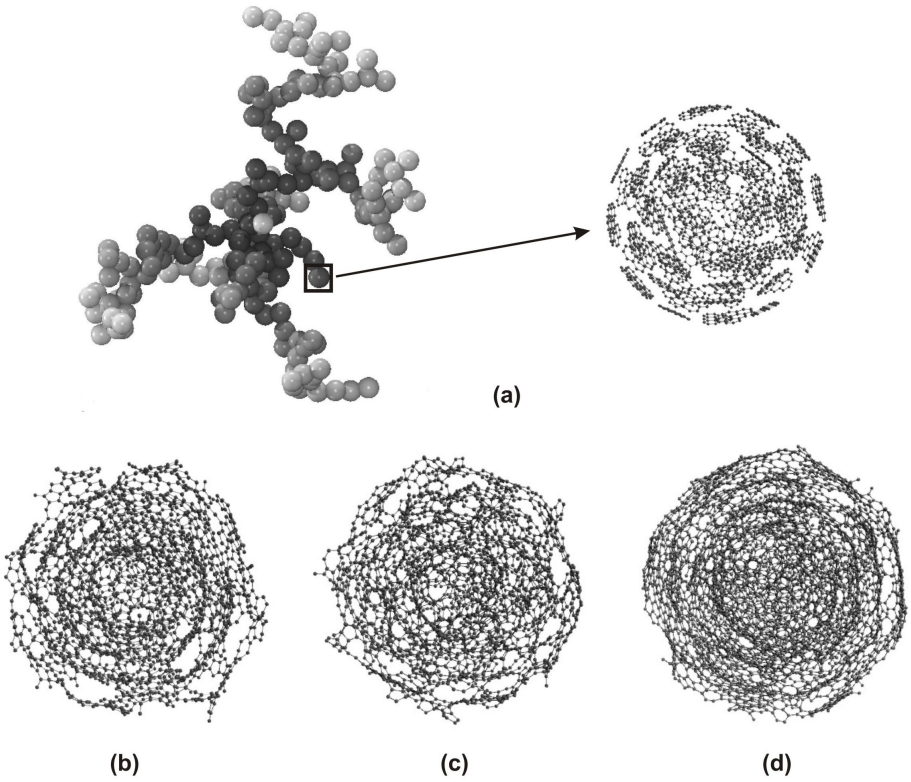

Figure 5: **(a) Simplified representation of a soot aggregate made of agglomerated primary nanoparticles with, on the right hand side of the figure, a picture of the the S_{units} nanoparticle containing 2147 C atoms that is used to model a primary nanoparticle of soot in the present approach. Additional models for these primary particles, based on the S_{holes} nanoparticles, are also shown at the bottom of the figure where (b), (c) and (d) correspond to S_{holes} nanoparticles containing 2133, 2206 and 3774 C atoms, respectively. See text for the definition of the S_{units} and S_{holes}** nanoparticles.

Of course, building models of **primary soot nanoparticles** as described above is completely arbitrary. Nevertheless, the nanoparticles generated this way present the main geometric characteristics of **primary soot nanoparticles** collected in flames[47] or emitted by aircraft[7], i.e., graphite-type layers arranged in an onion-like structure, although they are somewhat smaller (about $4 - 4.5$ nanometers of diameter here). Indeed, considering larger particles in our PDI calculations would be rather time consuming without any further approximations[14] and we thus choose to limit the present work to nanoparticles containing a relatively small number of carbon atoms.

Note that many different nanoparticles can be generated using our procedure. Here, we have restricted the calculations to four nanoparticles only, as an illustration of our approach. Moreover, as it will be shown below, this (limited) set of examples is nevertheless sufficient to show how the absorption properties can be related to the atomistic structure of soot nanoparticles.

4.2. Mass absorption coefficient of primary soot nanoparticles

In this section, we calculate the mass absorption coefficient for the four nanoparticles generated above and considered as independent nanoparticles. Indeed, we focus our attention on how spectroscopic information could be used to differentiate morphological information on soot nanoparticles at an atomistic scale. This differs from a lot of previous experimental and theoretical studies which were carried out by considering morphology dependence of absorption as a function of the fractal structures of soot aggregates, thus not considering **individual primary nanoparticles**[16, 52, 53, 54, 55].

The corresponding results are shown in Fig 6. Information concerning the geometrical characteristics of the nanoparticles considered as well as the position of the main peak in the MAC curves are given in Table 1 together with the calculated MAC values for three different wavelengths.

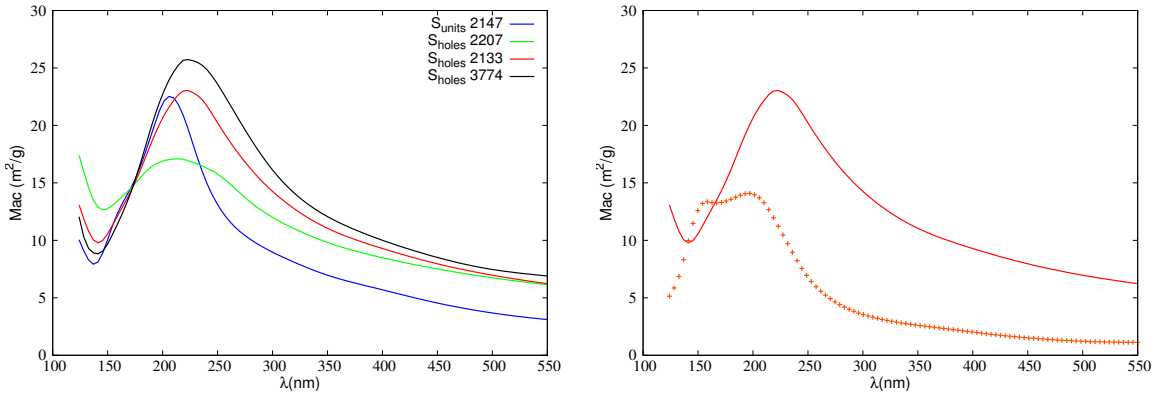

Figure 6: (a) MAC curves (in m^2/g) computed for various carbonaceous nanoparticles as a function of the wavelength (in nm). Blue, green, red and black curves correspond to S_{units} and S_{holes} with 2133, 2207, and 3774 carbon atoms, respectively. (b) Influence of the chemical composition on the S_{holes} (2133 C atoms) MAC curve : red and orange curves correspond to consideration of anisotropic (solid line) and isotropic (crosses) carbon polarizabilities in the calculations, respectively.

As shown in Fig. 6a, in the UV zone, the MAC curves for the soot nanoparticles are characterized by a large absorption peak, the maximum of which being shifted by about 20 nm from S_{units} to the largest S_{holes} (containing 3774 C atoms).

This can be related to what has been obtained for fullerenes, i.e., the position of the resonance peak is shifted to high wavelength values when the size of the nanoparticles increases. However, a shift of 7 nm is also obtained for two particles of similar size and built on a similar initial structure (S_{holes} containing 2207 and 2133 atoms). This indicates that not only the size but also the structure of the nanoparticle at the atomic level may strongly influence the position of the absorption peak.

In fact, a careful analysis of the differences between the **primary soot nanoparticles** considered here show that, besides size and number of atoms, these nanoparticles also differ by the ratio between isotropic and anisotropic carbons, i.e. carbons having three (anisotropic) or less than three (isotropic) nearest neighbors. Regarding this criterion, the maximum of the absorption peak shifts to higher wavelengths when increasing the number of anisotropic carbons. In other words,

because the anisotropic *vs.* isotropic character is defined here with respect to the graphite polarizability values (i.e., anisotropic carbons are characterized by the polarizability tensor of graphite atoms), such an effect in the absorption spectrum could be somehow related to the ratio between aromatic-like and aliphatic-like carbons in the nanoparticle.

structure	atoms	R_{in} (Å)	R_{out} (Å)	C_{iso}/C	peak position (nm)	Mac (250 nm) m^2/g	Mac (405 nm) m^2/g	Mac (550 nm) m^2/g
S_{unit}	2147	9.6	20.73	0.60	207	13.53	5.57	3.07
	2207	4.3	22.32	0.45	214	15.89	8.34	6.10
S_{hole}	2133	4.5	22.58	0.30	221	20.61	9.25	6.23
	3774	8.2	23.50	0.18	226	25.30	10.29	7.02

Table 1: Morphological details of the **primary soot nanoparticles** considered in the calculations and the corresponding computed MAC values for 3 different wavelengths. R_{in} corresponds to the radius of the internal cavity defined by the inner layer of the nanoparticle whereas R_{out} represents the radius of the nanoparticle, defined by its outer layer. Note that C_{iso}/C represent the proportion of C atoms represented by isotropic polarizabilities *vs.* the total number of C atoms in the nanoparticle.

To illustrate this influence on the MAC calculations, Fig. 6b shows the results obtained when considering only one specific **primary soot nanoparticle** (S_{holes} with 2133 atoms, for instance), but changing the parameters assigned to the carbon atoms. For illustration, we considered the limiting (unrealistic) case for which all carbons are represented by the same isotropic polarizability tensor (orange curve). The MAC spectrum obtained in this case strongly differs from the one calculated for the initial particle containing only 30 % of isotropic carbons (red curve). Indeed, it is characterized by a double peak, the maximum of which being shifted by 22 nm from the maximum calculated for the initial S_{holes} particle. This results clearly indicates that the chemical composition of the soot nanoparticle, modeled here by atoms with different types of polarizability tensors, may have a sufficiently strong influence on the MAC signals to allow detection of chemical differences by using spectroscopic measurements, especially in the spectral region of the resonance peak.

However, coming back to realistic nanoparticles (Fig. 6a) and regarding the MAC values at a given wavelength (and not only the position of the absorption peak at its maximum value), it clearly appears that the amplitudes of the differences calculated for different **primary soot nanoparticles** strongly depends on the spectral range. Indeed, Fig. 6a and values given in Table 1 for three different wavelengths clearly show that above about 350 nm, the MAC values are similar for the three S_{holes} nanoparticles which however differ by the size of their internal cavity, the number of carbon atoms and their ratio of isotropic to anisotropic carbons (i.e., their chemical composition). This indicates that, in this spectral region, differences in soot composition would not have any strongly visible influence on the MAC values. It should be noted however that differences in MAC values are evidenced between S_{holes} and S_{units} nanoparticles in this spectral range, without any clear and definite explanation for this results that may deserve more detailed investigations. S_{units} is indeed sligthly smaller than the other particles and it contains a very high proportion of graphite-type atoms (i.e., C atoms with 3 nearest neighbors). Anyway it does not correspond to any relaxed structure and, in that sense, this nanoparticle is certainly less realistic than the others. Anyway, our findings could be compared to the results issued from a compilation of various data indicating that, at 550 nm, there is a consistent mean value of 7.5 ± 1.2 m^2/g for the MAC of fresh light-absorbing carbon over a wide range of data available in the literature[16]. Interestingly, this value is not far from the one calculated here for the three S_{holes} nanoparticles (about 6.45 ± 0.5

m^2/g at 550 nm) whereas it is about twice that calculated for S_{units}.

Such a semi-quantitative agreement between our results based on an empirical modeling of **primary soot nanoparticles** and experimental or theoretical values obtained from other approaches reinforces the conclusion that, in this region of the spectrum, MAC values certainly do not significantly differ from one example of soot to another.

To summarize, the results obtained here indicate that MAC measurements could give information on the atomic details of soot nanoparticles only if they are performed in a well-suited wavelength range, i.e., at wavelengths typically between 200 and 350 nm (when considering the nanoparticles modeled here).

4.3. Comparison with analytical approaches

To evaluate the improvement given by the PDI approach and the atomistic description of the primary soot nanoparticles, we have also compared the results obtained in the present work with those calculated by using analytical models based on classical macroscopic electromagnetic theory, following the ideas of Michel et al[20].

First it should be noted that carbonaceous materials are strong absorbers of electromagnetic radiation and thus scattering is negliglible. As a consequence, the analytical approach can be restricted to exctinction properties that can be characterized by the extinction per volume calculated, for a spherical carbonaceous particle with a central empty void, as[48]

$$\eta_{ext} = 3kIm\left[\frac{(1-\rho)(\epsilon_\perp u_+ - 1)(\epsilon_\perp u_- - 1)}{(\epsilon_\perp u_- - 1)(\epsilon_\perp u_+ + 2) - \rho(\epsilon_\perp u_+ - 1)(\epsilon_\perp u_- + 2)}\right] \tag{7}$$

where

$$u_\pm = \pm\frac{\sqrt{1 + 8\epsilon_{//}/\epsilon_\perp} \mp 1}{2}; \rho = \left(\frac{R_{in}}{R_{out}}\right)^{u_+ - u_-} \tag{8}$$

and $\epsilon_\perp$ and $\epsilon_{//}$ are the parallel and perpendicular components of the dielectric tensor of carbon atoms in graphite, following the convention used in the present paper (see Section 2). R_{in} is the radius of the internal void whereas R_{out} represents the radius of the entire nanoparticle.

Two types of spherical particles have been considered for comparison between PDI and analytical approaches, namely the primary soot nanoparticles S_{holes} and S_{units} on the one hand and, on the other hand, the corresponding bucky-onions of fullerene that have been used to build these nanoparticles. The analytical calculations have been performed by considering spherical particles characterized by internal (R_{in}) and external (R_{out}) radii similar to those of the S_{holes}, S_{units} and buckyonions considered for the comparison. Moreover, in the analytical model, we have taken a carbon density equal to one carbon atom per 1.8788 Å^3, similar to that of graphite.

As it can be seen on Fig. 7a, the PDI and analytical approaches give very similar results when considering bucky-onion fullerenes. This first conclusion not only clearly

supports the accuracy of the PDI approach used here but also confirms that the analytical approach based on macroscopic electromagnetic theory could be safely used for modeling the optical answer of homogeneous spherical particules. In contrast, the MAC curves are significantly different when considering the more realistic S_{holes} and S_{units} primary soot nanoparticles, thus illustrating the role of the atomic defects in the structure of soot. Indeed, for these S_{holes} and S_{units} nanoparticles, both intensities and positions of the resonance peaks differ between the PDI and analytical approaches. More interestingly, for the S_{holes} nanoparticles (which are much less spherical than S_{units} due to the local rearrangement of the structure around defect sites upon optimization), MAC values at large wavelengths differ by almost a factor two between the two approaches, the values obtained using the PDI approach being much closer to the experimental measurements than the values given by the analytical approach.

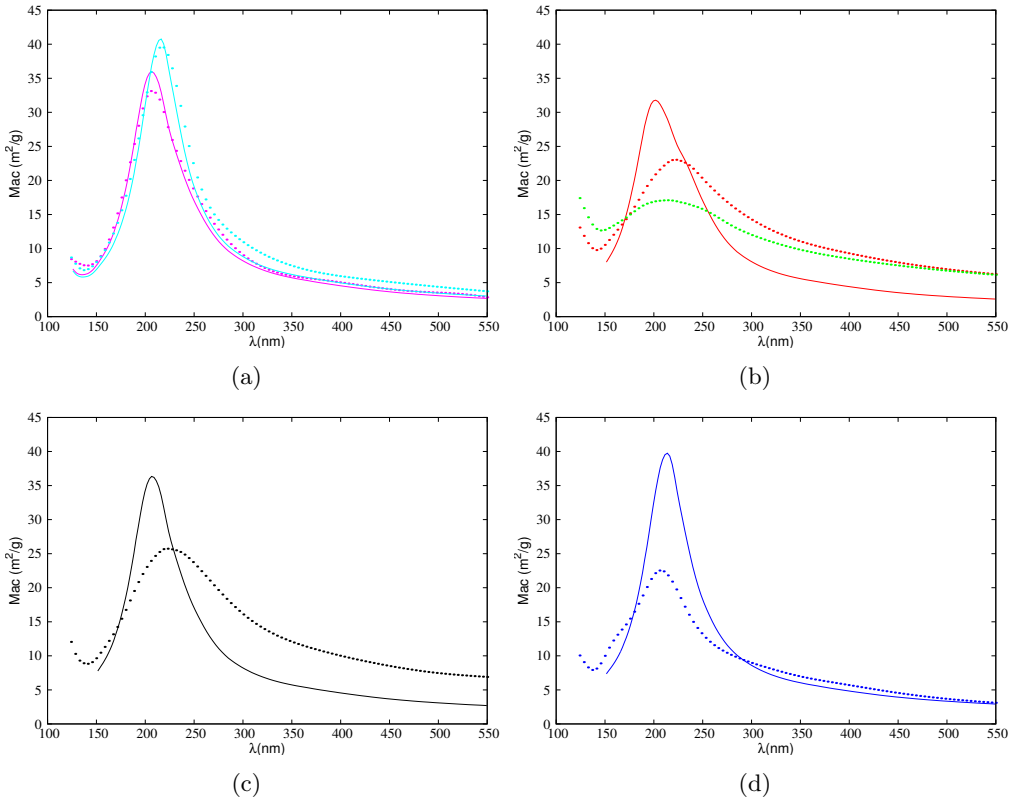

Figure 7: **Comparison between the MAC curves (in m^2/g) computed as a function of wavelength (in nm) by using either analytical (full curves) or PDI approach (dotted curves) for various carbonaceous nanoparticles : (a) Buckyonion $C240@C540@C960@C1500$ corresponding to S_{holes} containing either 2207 or 2133 atoms (pink curves) and buckyonion $C540@C960@C1500@C2160$ corresponding to S_{holes} containing 3774 atoms (light blue curves). (b) S_{holes} containing 2207 and 2133 atoms (green and red curves, respectively), (b) S_{holes} containing 3774 atoms (black curve), and (d) S_{units} containing 2147 atoms (blue curve).**

Such differences between the analytical and PDI approaches can be unambiguously related to the presence of defects in the atomistic structure of our soot models. They clearly emphasise the limits of the classical macroscopic electromagnetic theory for calculating the optical properties of defective structure that cannot be considered simply as homogeneous spherical particles.

Finally, it is interesting to note that such conclusions have been already reached in our previous work (Moulin et al., JQSRT 2008) although they were based on the calculations of the total polarizability of the nanoparticles for three incident energies, only.

4.4. Influence of the internal structure

In the previous section, we have considered onion-like particles of soot presenting an empty internal cavity defined, for instance for S_{holes}, by the size of the smallest embedded fullerene. In reality, the central region of the onion can be also filled with carbon atoms characterized by more or less well-organized structures[49, 50, 51]. The influence of such carbon nanostructures located inside the inner cavity has been studied theoretically by using analytical approaches and proved to have an important effect on the optical properties of the soot nanoparticle, depending on the disordered vs. crystalline character of these carbons[20, 48]. We thus used our approach to calculate the MAC of **primary soot nanoparticles** filled with various carbonaceous nanostructures, on the basis of an atomistic description of the corresponding particles.

For instance, we present here the results obtained when considering as initial structures the bukyonions $C540@C960@C1500$ and $C540@C960@C1500@C2160$ relaxed after removing 1157 and 1386 carbon atoms, respectively (an example of such nanoparticle is shown on Fig. 8). The MAC of these two particles has thus been calculated before and after adding at their center a small piece of graphite or an identical number of carbon atoms distributed on small dehydrogenated Polycyclic Aromatic Hydrocarbons (d-PAHs) randomly arranged at the center of the particles, for comparison. Note that we did not relax the final structure of the nanoparticles modeled this way, which have to be considered as ideal cases, only. An important feature to mention is that we choose geometries for the nanostructures embedded at the center of the nanoparticles that do not change the global ratio between anisotropic and isotropic C atoms (in other words, the ratio between C atoms having three nearest neighbors and the other C atoms).

The detailed information on these systems and the corresponding optical properties are given in Table 2 and their MAC curves are shown on Fig. 9. It is worth noting that the MAC curves calculated when considering well-ordered graphite and randomly scattered d-PAHs at the center of the nanoparticles do not exhibit any significant difference, and thus only the MAC curves corresponding to the former case are given in the Figure.

In contrast Fig.9 shows that including a carbonaceous nanostructure (graphite or d-PAHS) at the center of **a primary soot nanoparticle** leads to a shift to lower wavelengths (by 11 nm and 4 nm, respectively, for the two nanoparticles considered here) of the maximum of the MAC resonance peak. Lower MAC values are also calculated for the filled nanoparticles at high wavelengths (i.e., larger than about 220 nm). These conclusions are similar to those previously obtained, on the basis of analytical approaches, for the extinction curves of soot nanoparticles[20].

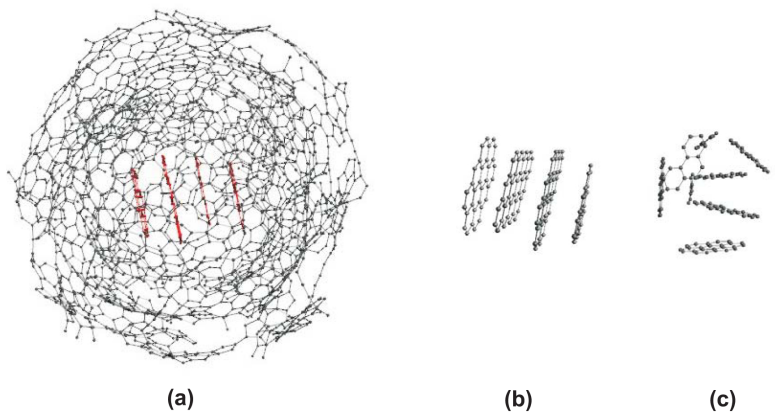

Figure 8: (a) Structure of the S_{holes} soot nanoparticle containing 1970 C atoms and including a small piece of graphite at its center (represented in red for clarity); (b) Example of a small piece of graphite that can been included at the center of the soot particles for the calculations of the MAC curves; (c) Example of randomly distributed small dehydrogenated Polycyclic Aromatic Hydrocarbons that can been included at the center of the soot particles for the calculations of the MAC curves.

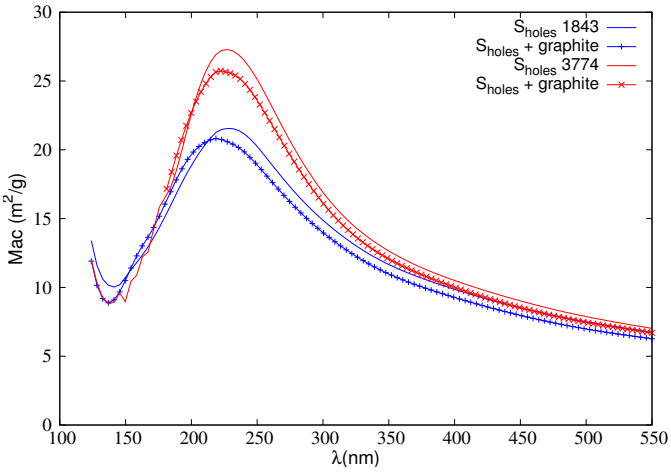

Figure 9: Comparison between the MAC curves (in m^2/g) computed as a function of wavelength (in nm) for two carbonaceous nanoparticles with (crosses) and without (solid lines) a small piece of graphite added at their center. Blue and red curves correspond to S_{holes} particles with 1843 and 3774 carbon atoms, respectively.

Considering that both the size and the ratio of isotropic *vs.* anisotropic carbons are the same for a given empty or filled nanoparticle, the shift and lowering of the MAC curves can be attributed to the filling of the inner part of the nanoparticles. The present results thus confirm that the characteristics of the **inner region of the primary soot nanoparticles** may significantly affect their optical properties. However, although the expected differences in the MAC curves might be used to discriminate between filled and empty particles, it appears that they cannot give unambiguous

structure	atoms	R_{in} (Å)	R_{out} (Å)	C_{iso}/C	peak position (nm)	Mac 250 nm m^2/g	Mac 405 nm m^2/g	Mac 550 nm m^2/g
	1843	9.5	22.58	0.34	229	19.97	9.73	6.74
	1970	–	22.58	0.34	218	18.68	9.14	6.27
S_{hole}	3774	8.2	23.50	0.18	226	25.30	10.29	7.02
	3888	–	23.50	0.19	222	23.41	10.12	6.70

Table 2: Morphological details of the **primary soot nanoparticles** considered in the calculations and the corresponding computed MAC values for 3 different wavelengths. R_{in} corresponds to the radius of the internal cavity defined by the inner layer of the nanoparticle whereas R_{out} represents the radius of the nanoparticle, defined by its outer layer Note that C_{iso}/C represent the proportion of C atoms represented by isotropic polarizabilities *vs.* the total number of C atoms in the nanoparticle.

information on the structuration of the carbon atoms inside the nanoparticles. In that sense, using atomistic simulations based on realistic force field models such as the AIREBO potential[46] used here could be of great interest to discriminate between different models of internal structure of soot nanoparticles, based on their relative stability in the calculations.

5. Conclusions

Here, we have used an atomistic approach to calculate the MAC curves of **carbonaceous particles modeling primary soot nanoparticles**. Our model is based on the knowledge of the atomic positions and polarizabilities inside the nanostructure under study. First, we have confirmed that the polarizability values coming from graphite data can be satisfactorily used to calculate the optical properties of round-shaped carbonaceous structures such as fulllerenes and carbon bucky-onions. Then, we have built various **primary soot nanoparticles** and compare their calculated MAC to study the influence of the atomistic characteristics of these nanoparticles on their optical properties.

The approach used here differs from the widely used implementations of the DDA method[22, 23] because it is based on the location of the atoms constituting the nanoparticles instead of on arbitrary chosen discretization volumes. This implies that the exact positions of the atoms inside the nanostructure and their atomic polarizability have to be known as input data of the calculations. But, it has the great advantage to give an exact route between these data and the optical characteristics of the nanoparticles considered. In other words, this method could be used to extract an atomistic information on such nanoparticles, from their optical characteristics.

This conclusion has been reinforced by comparing the results obtained using the PDI approach to those deduced from classical macroscopic eletromagnetic theory. Indeed, significant differences have been evidenced between the PDI and analytical approaches as soon as defects are introduced in the atomistic structure of the primary nanoparticles of soot, that thus cannot be considered simply as homogeneous spherical particles.

Our results clearly show that the chemical composition of the nanoparticle may have a sufficiently strong influence on the MAC curves to allow detection of chemical differences by using near UV-visible spectroscopic measurements. However, MAC measurements could give information on the atomic details of the nanoparticles only if they are performed in a well-suited wavelength range, i.e., at wavelengths typically between 200 and 350 nm. In a more general way, our calculations show

that MAC values as well as differences between MAC curves corresponding to different nanoparticles may strongly vary with wavelength. In that sense, measurements at a given wavelength only is certainly not representative of the whole curves and thus should be considered with caution.

Moreover, soot is made of aggregates rather than of isolated primary nanoparticles and, from an experimental point of view, the measured optical properties could also depend on the size, shape and fractal dimension of these aggregates. In addition, not only absorption but also extinction properties could be used to get more information on the characteristics of soot. Indeed, it has been recently shown, on the basis of comparison between experimental measurements and T-matrix calculations, that mass extinction cross sections (MEC) are much sensitive to aggregate morphology than MAC measurements[54] although this conclusion is quite controversial because it appears contrary to recent modeling studies where both MAC and MEC displayed morphology dependence[53]. Using the PDI model we calculate, few years ago, the electric permittivities of soot aggregates, showing that the dominant effect governing permittivity variations with energy is the chemical composition of the primary particles rather than the fractal dimension of the aggregate[14]. The translation of this conclusion in terms of absorption and extinction properties of soot aggregates certainly deserves detailed investigations, in connection with the controversy mentioned above[53, 54]. Calculations of MAC and MEC curves for aggregates of primary particles are thus in progress.

Finally, it is worth mentioning that carbonaceous particles in the Troposphere can be rapidly surrounded by other species, especially water molecules, after their emission. Provided that the dynamic polarizability tensors of the adsorbed atoms/molecules is known, the present method could be easily used to quantify the influence of aging on the soot optical characteristics.

Acknowledgements

The Authors thank the French Embassy in La Havana and the Region de Franche-Comté for their financial support. Some computations have been performed on the supercomputer facilities of the Mésocentre de calcul de Franche-Comté. Fruitful discussions with Prof. JC Rayez (ISM-Bordeaux) on the atomic polarizabilities of carbon atoms are gratefully acknowledged.

[1] Chung, SH, Seinfeld JH. Global Distribution and Climate Forcing of Carbonaceous Aerosols. J Geophys Res 2002;107:4407.

[2] Haywood J, Boucher O. Estimates of the direct and indirect radiative forcing due to tropospheric aerosols. A review. Rev Geophys 2000;38:513-43.

[3] Lohmann U, Feichter J. Global indirect aerosol effects: a review. Atmos Chem Phys 2005;5:71537.

[4] Fuzzi S, Andreae MO, Huebert BJ, Kulmala M, Bond TC, Boy M, Doherty SJ, Guenther A, Kanakidou M, Kawamura K, Kerminen VM, Lohmann U, Russell LM, Pöschl U. Critical assessment of the current state of scientific knowledge, terminology, and research needs concerning the role of organic aerosols in the atmosphere, climate, and global change. Atmos Chem Phys 2006;6:201738.

[5] Chen Y, Penner JE. Uncertainty Analysis for Estimates of the First Indirect Aerosol Effect. Atmos Chem Phys 2005;5:2935-48.

[6] Combustion Generated Fine Carbonaceous Particles. Bockhorn H, D'Anna A, Sarofim AF, Wang H, editors. Karlsruhe: KIT Scientific Publishing; 2009.

[7] Demirdjian B, Ferry D, Suzanne J, Popovicheva OB, Persiantseva NM, Shonija NK. Heterogeneities in the Microstructure and Composition of Aircraft Engine Combustor Soot: Impact on the Water Uptake. J Atmos Chem 2007;56:83-103.

[8] Violi A. Modeling of Soot Particle Inception in Aromatic and Aliphatic Premixed Flames. Combust Flame 2004;139:279-87.

[9] Moulin F, Picaud S, Hoang PNM, Partay L, Jedlovszky P. A grand canonical Monte Carlo simulation study of water adsorption on a model soot particle. Mol Sim 2006;32:487-493.

[10] Moulin F, Picaud S, Hoang PNM, Partay LB, Jedlovszky P. A Grand Canonical Monte Carlo simulation of the aggregation of water molecules on chemically modified soot particles. Comp Lett 2008;4:105-16.

[11] Oubal M, Picaud S, Rayez MT, Rayez JC. Water adsorption on oxidized single atomic vacancies present at the surface of small carbonaceous nanoparticles modeling soot. Chem Phys Chem 2010;11:4088-96.

[12] Hantal G, Picaud S, Hoang PNM, Voloshin VP, Medvedev NN, Jedlovszky P. Water adsorption isotherms on porous onion-like carbonaceous particles. Simulations with the Grand Canonical Monte Carlo method. J Chem Phys 2010;133:144702.

[13] Moulin F, Devel M, Picaud S. Optical properties of soot nanoparticles. J. Quant. Spectrosc. Radiat. Transfer 2008;109:1791-1801.

[14] Langlet R, Vanacharla MR, Picaud S, Devel M. Bottum-up multi-step approach to study the relations between the structure and the optical properties of carbon soot nanoparticles. J. Quant. Spectrosc. Radiat. Transfer 2009;110:1615-27.

[15] Sorensen CM. Light scattering by fractal aggregates: A review. Aerosol Sci Technol 2001;35:648-87.

[16] Bond TC, Bergstrom R. Light absorption by carbonaceous particles: an investigative review. Aerosol Sci Technol 2006;40:27-67.

[17] Mie G. Beiträge zur Optik Trüber Medien, Speziell Kolloidaler Metallösungen. Annalen der Physik 1908;25:377-445.

[18] Bohren CF, Huffman DR. Absorption and scattering of light by small particles. 1983. John Wiley and Sons, New York.

[19] Keller D, Bustamante C. Theory of the interaction of light with large inhomogeneous molecular aggregates. I. Absorption. J Chem Phys 1986;84:2961-71.

[20] Michel B, Henning Th, Jäger, Kreibig U. Optical extinction by spherical carbonaceous particles. Carbon 1999;37:391-400.

[21] Michel B. Statistical method to calculate extinction by small irregularly shaped particles. J Opt Soc Am 1995;12:2471-81.

[22] Purcell EM, Pennypacker CR. Scattering and Absorption of Light by Nonspherical Dielectric Grains. Astrophys J 1973;186:705-14.

[23] Draine BT. The Discrete-Dipole Approximation and its Application to Interstellar Graphite Grains. Astrophys J 1988;333:848-72.

[24] Draine BT, Flatau PJ. Discrete dipole approximation for scattering calculations. J Opt Soc Am A 1994;11:1491-99.

[25] Mishchenko MI, Travis LD, Mackowski DW. T-matrix computations of light scattering by nonspherical particles: A review. J Quant Spectrosc Radiat Transfer 1996;55:535-75.

[26] Applequist J, Carl JR, Fung K-K. An Atom-Dipole Interaction Model for Molecular Polarizability, Application to Polyatomic Molecules and Determination of Atom Polarizabilities. J Am Chem Soc 1972;94:2952-60.

[27] McDonald J, Golden A, Jennings G. OpenDDA: a novel high-performance computational framework for the discrete dipole approximation. Int J High Perf Comp Appl 2009;23: 4261

[28] Yurkin MA, Hoekstra AG. The discrete-dipole-approximation code ADDA: capabilities and known limitations. J. Quant. Spectrosc. Radiat. Transfer 2011;112: 223447.

[29] Choliy VY. The discrete dipole approximation code DDscat.C++: features, limitations and plans. Adv Astron Space Phys 2013;3: 6670.

[30] Devel M, Girard C, Joachim C. Computation of electrostatic fields in low-symmetry systems: application to STM configurations. Phys Rev B 1996;53:13159-68.

[31] Draine BT, Lee HM. Optical properties of interstellar graphite and silicate grains. Astrophys J 1984;285:89-108.

[32] Laor A, Draine BT. Spectroscopic constraints on the properties of dust in active galactic nuclei. Astrophys J 1993;402:441-68.

[33] Draine BT. Scattering by interstellar dust grains. II. X-rays. Astrophys J 2003;598:1026-37.

[34] Djurisik A, Li EH. Optical properties of graphite. J Appl Phys 1999;85:7404-10.

[35] Senet P, Henrard L, Lambin P, Lucas AA. A one parameter model of the UV spectra of carbon. In: Kuzmany H, Fink J, Lehring M, Roth S, editors. Proceedings of the international winterschool on electronic properties of novel materials. Progress in fullerene research, vol. 393. Singapore: World Scientific; 1994.

[36] Andersen J, Bonderup E. Classical dielectric models of fullerenes and estimation of heat radiation. Eur Phys J D 2000;11:435-48.

[37] Sohmen E, Fink J, Krätschmer W. Electron energy-loss spectroscopy studies on C_{60} and C_{70} fullerite. Z Phys B - Condensed Matter 1992;86:87-92.

[38] Kuzuo R, Terauchi M, Tanaka M, Saito Y, Shinohara H. Electron-energy-loss spectra of crystallite C_{84}. Phys Rev B 1994;49:5054-57.

[39] Saito S, Oshiyama A. Cohesive Mechanism and Energy Bands of Solid C_{60}. Phys Rev Lett 1991;66:2637-40.

[40] Smith AL. Comparison of the ultraviolet absorption cross section of C_{60} buckminsterfulleren in the gas phase and in hexane solutions. J Phys B 1996;29:4975-80.

[41] Berkowitz J. Sum rules and the photoabsorption cross sections of C_{60}. J Chem Phys 1999;111:1446-53.

[42] Iglesias-Groth S. Fullerenes and buckyonions in the interstellar medium. Astrophys J 2004;608:L37-L40.

[43] Mayer A, Lambin Ph, AAstrand PO. An electrostatic interaction model for frequency-dependent polarizability: methodology and applications to hydrocarbons and fullerenes. Nanotechnology 2008;19:025203.

[44] Andreae MO, Gelencsér A. Black carbon or brown carbon? The nature of light-absorbing carbonaceous aerosols. Atmos Chem Phys 2006;6:3131-48.

[45] Shaddix CR, Williams TC. Soot structure and dimensionless extinction coefficient in diffusion flames: implications for index of refraction. In Bockhorn H, D'Anna A, Sarofim AF and Wang H, editors. Combustion Generated Fine Carbonaceous Particles. KIT Scientific Publishing; 2009: pp. 17-33.

[46] Stuart SJ, Tutein AB, Harrison JA. A reactive potential for hydrocarbons with intermolecular interactions. J Chem Phys 2000;112:6472-6486.

[47] Grieco WJ, Howard JB, Rainey LC, Van der Sande JB. Fullerenic carbon in combustion-generated soot. Carbon 2000;38:597-614.

[48] Henrard L, Lucas AA, Lambin Ph. On the 2175 Åabsorption band of hollow, onion-like carbon particles. Astrophys J 1993;406:92.

[49] de Heer WA, Ugarte D. Carbon onions produced by heat treatment of carbon soot and their relation to the 217.5 nm interstellar absorption feature. Chem Phys Lett 1993;207:480-86.

[50] Banhart F, Ajayan PM. Carbon onions as nanoscopic pressure cells for diamond formation. Nature 1996;382:433-35.

[51] Popovicheva OB, Persiantseva NM, Kuznetsov BV, Rakhmanova TA, Shonija NK, Suzanne J, Ferry D. Microstructure and water absorbability of aircraft combustor soots and kerosene flame soots: toward an aircraft-generated soot laboratory surrogate. J Phys Chem A 2003;107:10046-54.

[52] Liu L, Mishchenko MI, Arnott WP. A study of radiative properties of fractal soot aggregates using the superposition T-matrix method. J Quant Spectrosc Radiat Transfer 2008;109:2656-63.

[53] Scarnato BV, Vahidinia S, Richard DT, Kirchstetter TW. Effects of internal mixing and aggregate morphology on optical properties of black carbon using a discrete dipole approximation model. Atmos Chem Phys 2013;13:5089-101.

[54] Radney JG, You R, Ma X, Conny J, Hodges JT, Zachariah MR, Zangmeister CD. Dependence of Soot Optical Properties on Particle Morphology: Measurements and Model Comparisons. Environ Sci Technol 2014;48:3169-76.

[55] Prasanna S, Rivire Ph, Soufiani A. Effect of fractal parameters on absorption properties of soot in the infrared region. J Quant Spectrosc Radiat Transfer 2014;148:141-55.